Available online at www.sciencedirect.com
ScienceDirect
Trans. Nonferrous Met. Soc. China 24(2014) s81−s89
Transactions of Nonferrous Metals Society of China
www.tnmsc.cn

Effect of concentration of ATH on mechanical properties of polypropylene/aluminium trihydrate (PP/ATH) composite

Atta ur Rehman SHAH[1], Dong-woo LEE[1], Yi-qi WANG[1], Abdul WASY[1], K. C. HAM[2], Krishnan JAYARAMAN[3], Byung-Sun KIM[4], Jung-Il SONG[1]

1. Department of Mechanical Engineering, Changwon National University, Changwon, Korea;
2. Department of Mechanical Engineering, Inha Technical College, Korea;
3. Department of Mechanical Engineering, University of Auckland, New Zealand;
4. Composite Research Center, Korea Institute of Materials Science (KIMS), Korea

Received 18 June 2013; accepted 28 November 2013

Abstract: Aluminium trihydrate (ATH) is being extensively added to polypropylene (PP) to make a fire retardant composite. Blends of PP/ATH composite are more fire resistant as compared to pure PP. Percentage proportion of both the constituents in the final composite depends upon the application. Improvement in the fire retardant properties of such composites have been studied and published in literature but effects on mechanical strength have not been addressed. The effect of concentration of ATH on the strength of PP/ATH composite was presented. The tensile, flexural and fracture properties were studied and discussed. Experimental tests, ASTM analytical formulae and finite element approach were used. It has been found that increase in ATH has an inverse effect on the mechanical strength.

Key words: aluminium trihydrate; polypropylene; composite; fire retardant; fracture toughness; mechanical strength

1 Introduction

Thermal and fire retardant properties of polymers often can be altered through the introduction of particulate fillers. These fire retardant polymers have robust application in various fields, such as aerospace, automotive, marine, military [1,2]. Polypropylene (PP) is a thermoplastic polymer which is being used in various industries including textile, stationary, automotive, laboratory equipment, plastic parts and reusable containers of various types [3]. Different concentrations of ATH are commonly added to PP for different applications to increase its flame Refs. [4]. Thermal, electrical and fire retardant properties of ATH blended with different polymers including PP have already been published in Refs. [4−12], while not enough information is available on the mechanical strength and fracture toughness of these polymer composites.

This work includes a study to calculate tensile strength, flexural strength and fracture toughness of a PP/ATH composite. Different blends of the composite with varying amounts of the ATH have been analyzed and effects of ATH on the final strength of the composite have been studied. Simple uniaxial tensile test is run to find the tensile properties while a three-point bending test according to ASTM standard is carried out to calculate the flexural strength. The bending specimen is then modeled and analyzed with finite element technique and it is found that the finite element analysis gives almost the same results as the experimental test, hence the model is validated. The fracture toughness of the same model has been calculated using FE technique and SENB (single edge notched beam) formulae of ASTM. It is observed that with the increase of ATH in the blend, the mechanical strength and fracture toughness of the composite are decreasing.

2 Composite preparation

PP and ATH are the two basic constituents of the composite. Different amounts of ATH are added to PP to

Foundation item: Projects (2012-0009455; 2012-0008302) supported by the National Research Foundation of Korea (NRF) Grant Funded by the Korea Government (MEST)
Corresponding author: Jung-Il SONG; Tel: +82-55-2135406; E-mail: jisong@changwon.ac.kr
DOI: 10.1016/S1003-6326(14)63292-1

make different compositions and study the effect of ATH in the composite. Maleic anhydride grafted polypropylene (MAPP) is also added to the composite as a coupling agent which is a renowned agent to improve the interface bonding between both the constituents [13]. Firstly, the PP, ATH and MAPP are put in one bag and shaken well to mix. The mixture is then put into the extruding machine, and extrusion is carried out at 210−220 ℃ [14]. After extrusion, it is cut into small pallets. These small pellets are then put into the injection molding machine. Dog-bone shape specimens of the required dimensions for experimental testing are obtained from the injection molding process. The manufacturing process flow chart is explained in Fig. 1, while the blends compositions of the three constituents are shown in Table 1.

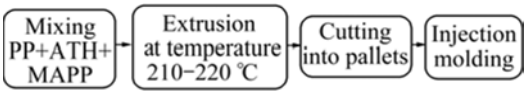

Fig. 1 Flow chart of manufacturing process

Table 1 Concentration of constituents in different blends

w(PP)/%	*w*(ATH)/%	*w*(MAPP)/%	*w*(Total)/%
100	−	−	100
93	5	2	100
88	10	2	100
83	15	2	100
48	50	2	100

3 Experimental

3.1 Tensile test

Tensile test of the PP/ATH composite specimen has been performed using (Instron 5567) 30 kN load cell. Specimen geometry and experiment were setup according to ASTM standard D638 for tensile tests. The dog-bone shape specimen for tensile specimen is shown in Fig. 2.

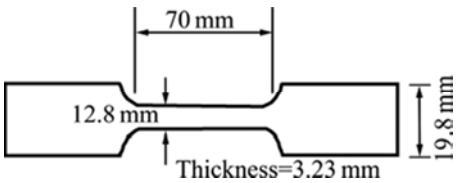

Fig. 2 Dog-bone specimen for tensile test

3.2 Bending test

Three-point bending test has been run according to the specifications recommended in ASTM standard D790 using a load cell of 5 t manufactured by R & B Unitech M, Korea. The dimensions and orientation of the rectangular bending specimen are shown in Fig. 3, where L is the span length between the two supports, d is the depth and b is the thickness of the specimen.

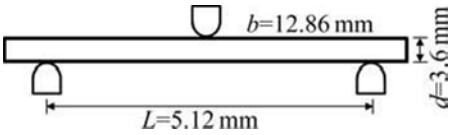

Fig. 3 Three-point bending test setup

4 Finite element modeling

4.1 Three-point bending analysis

A three-dimensional geometric model is made with the same dimensions and geometry which was used in the experimental three-point bending tests. The flexural stress formula for a three-point bending specimen available in the ASTM standard D790 is:

$$\sigma_f = 3PL/(2bd^2) \quad (1)$$

where σ is the stress in the outer fiber at midpoint; L is the span length; P is the load applied; b is the beam width; d is the depth of beam. Length, width and depth used in the above formula are already known to us. The flexural strength (obtained from experimental bending test) is put in Eq. (1), and the maximum load P for the three-point bending specimen can be obtain. By using the same value of P in the FEA, bending stress is calculated for each blend of the PP/ATH composite. The stress values obtained from FE technique are compared with those obtained from experimental bending tests to validate the FE model.

4.2 Fracture analysis

Fracture analysis of the PP/ATH composite has been carried out using FE technique on a specimen according to ASTM standard E1290 as shown in Fig. 4. A single edge notched beam (SENB) specimen of span length 51.2 mm, depth 12.86 mm and width 6.43 mm was modeled with a crack size of 7.3945 mm. This crack size and shape are decided as recommended by the ASTM standard. This is a plane strain fracture mechanics problem. Standard formula to calculate fracture toughness K_{IC} is:

$$K_{IC} = \frac{P}{(BW)^{1/2}}(Y) \quad (2)$$

where B is the width; W is the depth of the beam, which are already known; P is the load when stress at crack tip reaches the flexural strength of the material, and P is calculated by FEA of the SENB; Y is the geometric factor which can be calculated from the following

Fig. 4 Geometric model for fracture analysis according to ASTM E1290

expression:

$$Y=\frac{1}{(1-a_0/W)^{3/2}}[(2+a_0/W)(0.886+4.64_{a_0}/W-13.32(a_0/W)^2+14.72(a_0/W)^3-5.6(a_0/W)^4] \quad (3)$$

where a_0 is the initial crack size, which is 7.3945 mm.

Material properties of the composite used in the FE analysis are taken from the experimental tests above.

5 Experimental results

5.1 Tensile test

Figure 5 shows stress−strain curves for different blends of PP/ATH composite. It is observed that tensile strength of the composite is decreasing with the increase of ATH in the blend. Pure PP is stronger than the PP/ATH composite. On the other hand, elastic modulus is seen to increase slightly with the addition of more ATH in the composite. This decrease in the strength is

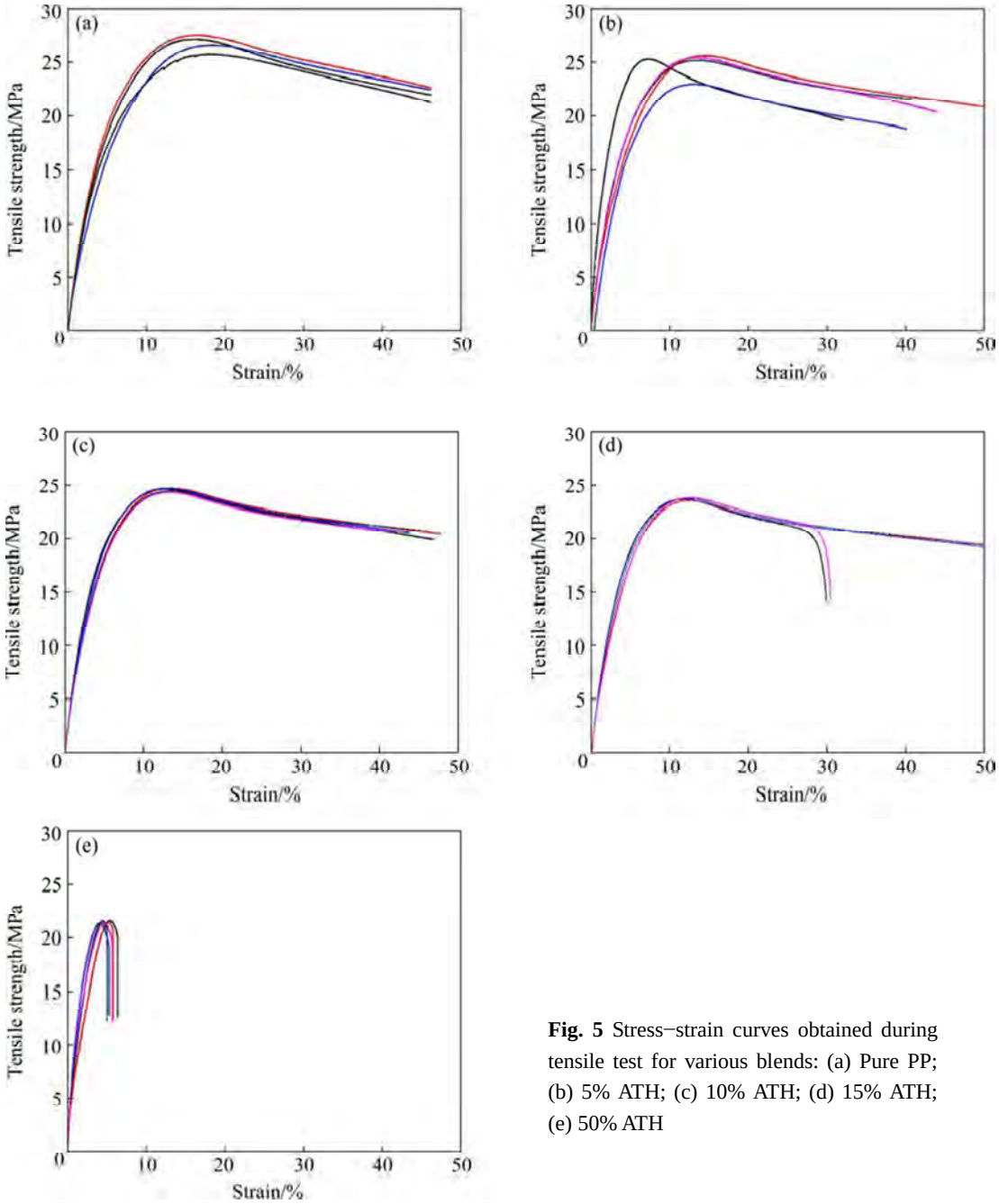

Fig. 5 Stress−strain curves obtained during tensile test for various blends: (a) Pure PP; (b) 5% ATH; (c) 10% ATH; (d) 15% ATH; (e) 50% ATH

because of the week intermolecular forces between PP and ATH. The average values of tensile strength, elastic modulus and elongation at breakup for each blend of PP/ATH composite found in this case are listed in Table 2 and plotted in the bar chart in Fig. 6. Pure PP and all the blends of PP/ATH composites are compared for their tensile strength and elastic modulus. It can be seen that pure PP has the maximum tensile strength while 50% ATH mixed with PP has the maximum elastic modulus.

Table 2 Tesile properties of pure PP and PP/ATH composites

Blend of PP/ATH	Tensile strength/MPa	elastic modulus/GPa	Elongation at breakup/%
Pure PP	26.80	1.678	46.0587
5% ATH	25.00	1.671	41.5081
10% ATH	24.42	1.762	45.4543
15% ATH	23.82	1.829	46.7580
50% ATH	21.32	3.245	5.6565

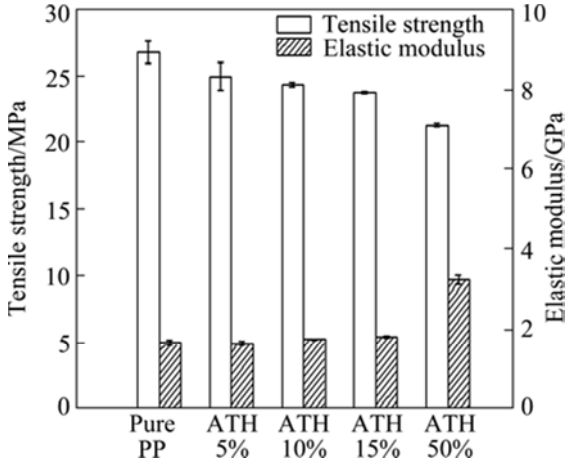

Fig. 6 Variation in tensile strength and elastic modulus among different blends of PP/ATH

5.2 Three-point bending test

Three-point bending test was performed according to the setup mentioned earlier. Flexural strength vs. time curves are obtained as shown in Fig. 7. It is observed that flexural strength of the composite is decreasing with the increase of ATH in the blend. Also the time to reach the maximum stress is low for composite having higher amount of ATH compared with those which contain smaller amount of ATH. It means the intermolecular force in broken easily in the composites which have higher amount of ATH. Figure 8 shows comparison of the flexural strengths of all blends of PP/ATH composite. It can be seen that the blend having 5% ATH has a highest flexural modulus while blend having 50% ATH

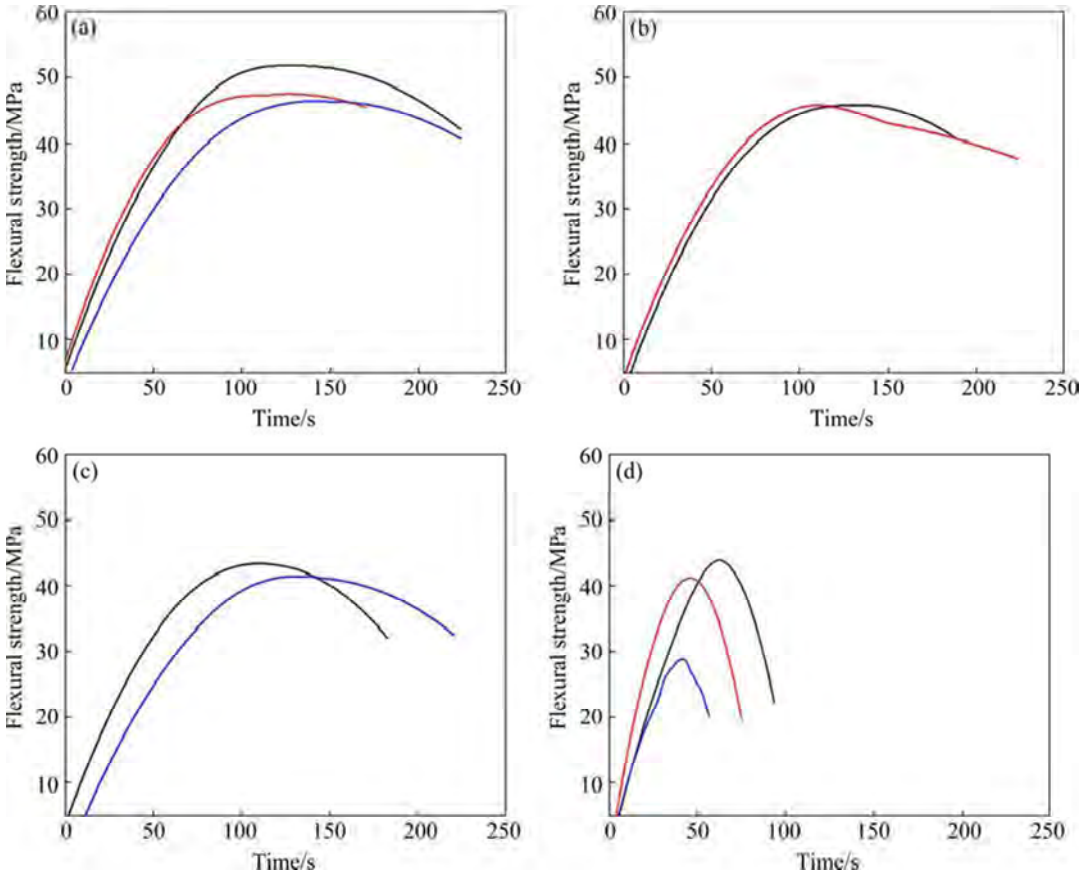

Fig. 7 Flexural strength vs time plot for various blends of PP/ATH composite: (a) 5% ATH; (b) 10% ATH; (c) 15% ATH; (d) 50% ATH

has a lowest flexural strength. Average numerical values of flexural strength of all blends are listed in Table 3.

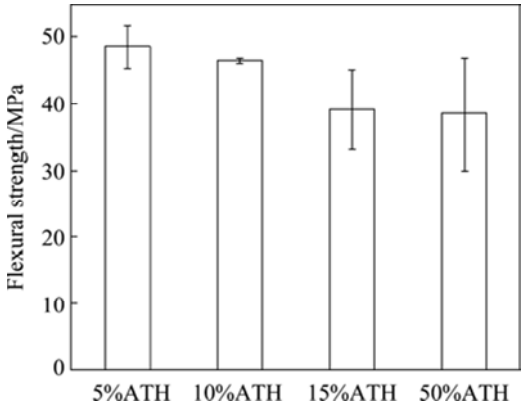

Fig. 8 Variation in flexural strength of different blends of PP/ATH

Table 3 Flexural strength of PP/ATH composites

Blend of PP/ATH	Flexural strength/MPa
5% ATH	48.53
10% ATH	46.55
15% ATH	39.21
50% ATH	38.45

5.3 Surface morphology

The strength of the composite decreases with the addition of ATH because of the bonding between PP and ATH particles. To study this effect, SEM (scanning electron microscopy) images have been obtained. SEM images explain the surface topography and composition in details. SEM images of all specimens were taken with different zooming scales. Figure 9 shows these images before the application of any load. The images are taken at the cross sections of the polished specimens. Figure 9(a) shows the PP+5% ATH specimen and its surface can be seen with the minimum number of flaws. As soon as the amount of ATH is increased, the surface flaws increase as shown in Fig. 9. These surface flaws are because of the week interface bonding between the PP and ATH particles.

The flaws are maximum in the last case including 50% ATH. Hence ATH is acting as an impurity for the strength, and this is the reason why the mechanical strength of the composite is decreasing with the increase of the ATH. This phenomenon has already been observed in the tensile and bending test results above.

As a result of flexural loading all the specimens got permanent bending deformations but none of them got broken except the specimen with 50% ATH. The last

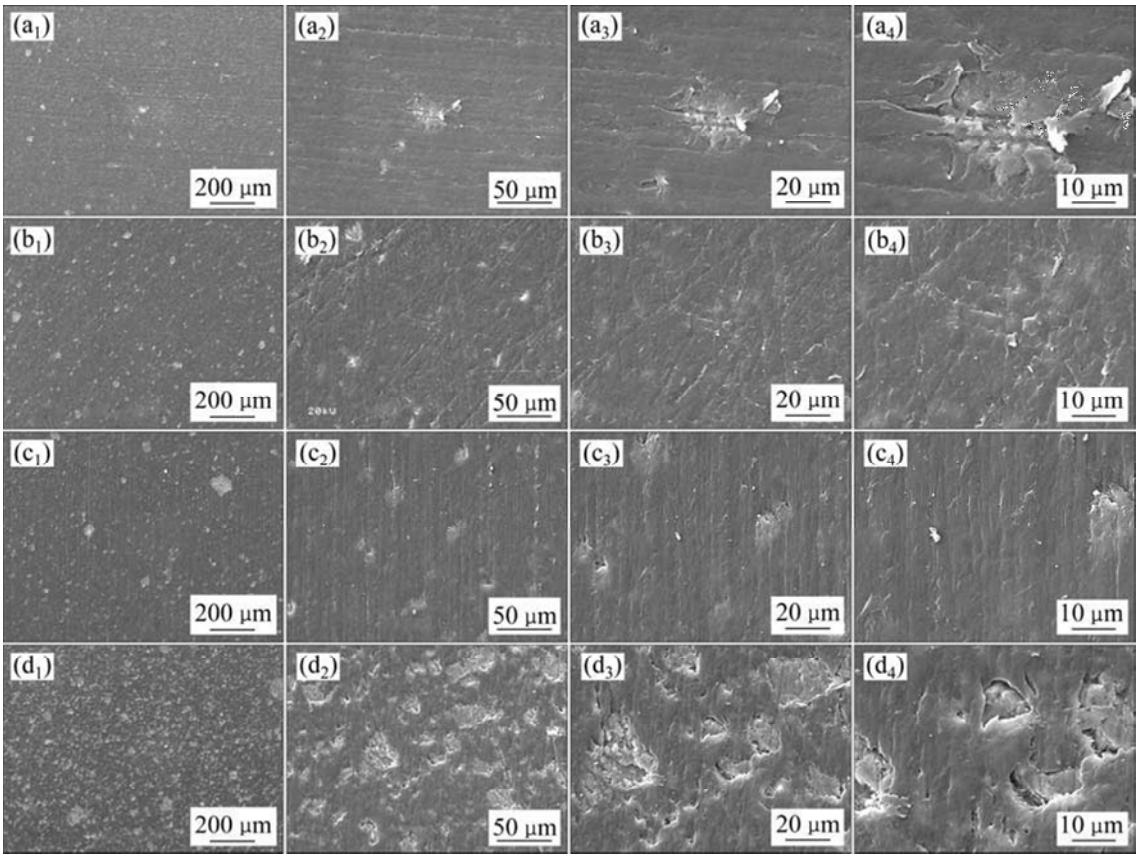

Fig. 9 SEM images of PP/ATH composite specimens before loading: (a_1)−(a_4) PP+5%ATH; (b_1)−(b_4) PP+10%ATH; (c_1)−(c_4) PP+15%ATH; (d_1)−(d_4) PP+50%ATH

specimen which has 50% ATH got come apart into two pieces. It shows that specimen with 50% ATH is more brittle, and brittleness is increasing with the increase of ATH. The real camera picture of the specimens is shown in Fig. 10. It can be seen that only the last specimen which contains 50% ATH has been broken. To study the fractured surface topology of this specimen, SEM images have been taken at the fractured cross section of the 50% ATH specimen.

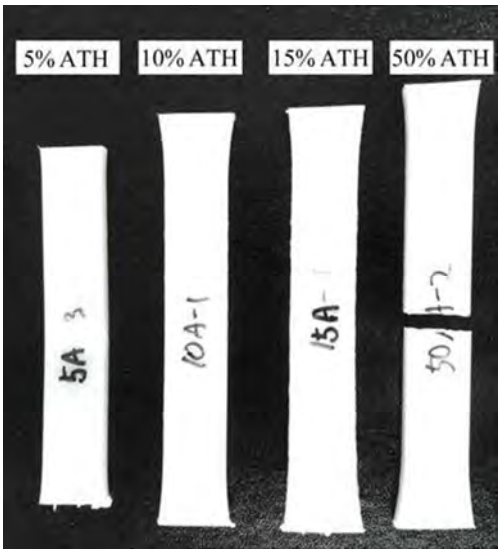

Fig. 10 Camera image of specimens after bending test

Figure 11 shows SEM images of 50% ATH specimen before and after fracture. It can be seen from Figs. 11(a_1, a_2) that surface has no prominent flaw in the non-fractured image as it's polished, but in the fractured image the surface flaws can be observed clearly. As soon as the resolution is being increased, the surface is becoming more visible. In Figs. 11(b_1, b_2) and (c_1, c_2), the week interface between PP and ATH molecules is clearer than the first case. In Figs. 11(d_1, d_2), week interface bonding can be clearly observed. PP and ATH molecules have some interface gaps and they are not perfectly bonded. This week bonding is causing reduction in its strength and making it more brittle and hence this specimen was broken under bending loading. Hence, SEM images explain clearly the reason of reduction of the strength with the increase of ATH as observed in the experimental results above.

6 FEA results

6.1 Model validation

Finite element analysis is an effective approach for engineers to overcome experimental limitations. But it is very important to validate the FE model by comparing some results with the known experimental or analytical solutions. If the values of FEA and experimental tests are close to each other, we can proceed to run any other analysis on that model with the same mesh size. In this study, the three-point bending test is performed experimentally and then repeated with FE technique. It is observed that FEA results agree well to the experimental results within an error limit of 5% which is acceptable. Analysis is performed with various mesh sizes and it was found that a quadrilateral mesh with 0.5 edge size gives better results with a minimum.

The bending stresses obtained from FEA and shown in Fig. 12 are very close to the experimental values listed in Table 4. An average error of 5% exists between the FE results and the corresponding experimental results, which is acceptable. The applied load P calculated from Eq. (1) and bending stress from FEA and experimental tests are listed in Table 4. A comparison of the results of the two separate techniques is plotted in Fig. 13, where it can be seen that they are very close to each other and have the same trend. Since the FEA results agree to the

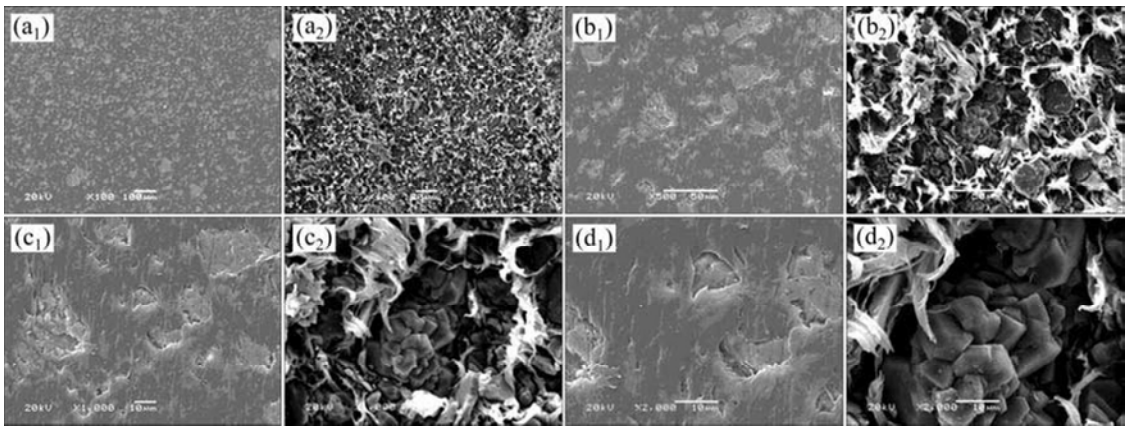

Fig. 11 SEM images of fracture (50% ATH) specimen before loading (a_1, b_2, c_3, d_4) and after fracture (a_2, b_2, c_2, d_2): (a_1, a_2) 100x resolution; (b_1, b_2) 500x resolution; (c_1, c_2) 1000x resolution; (d_1, d_2) 2000x resolution

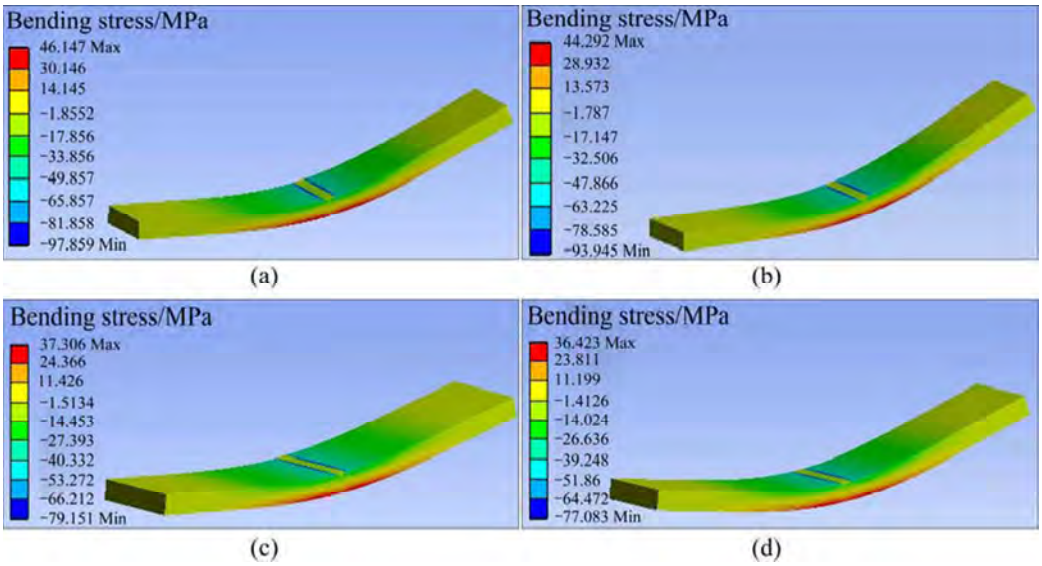

Fig. 12 FE plots of bending stress in PP/ATH composite of different blends: (a) 5% ATH; (b) 10% ATH; (c) 15% ATH; (d) 50% ATH

experimental results, the model is validated, and the FEA technique can be used for the fracture analysis in the next section.

Table 4 Comparison of FEA and experimental results

Blend of PP/ATH	Applied load *P*/N	Bending stress/MPa		Error/%
		Experimental	FEA	
5% ATH	83.16	48.54	46.15	4.90
10% ATH	79.82	46.55	44.29	4.85
15% ATH	67.23	39.21	37.31	4.86
50% ATH	65.62	38.45	36.42	5.26

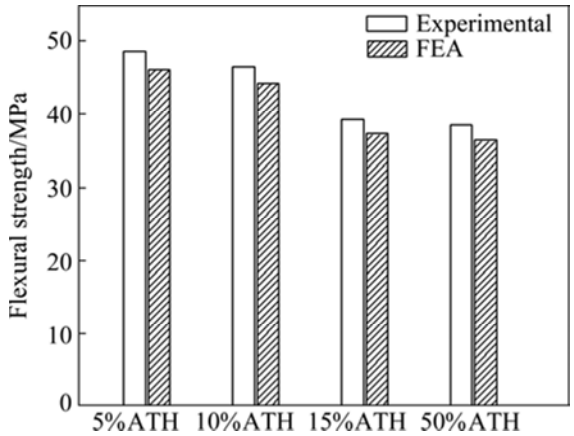

Fig. 13 Comparison of FE and experimental values of flexural stress

6.2 Fracture analysis

Equation (2) is used to calculate the fracture toughness of the specimen shown in Fig. 4. The critical load P in Eq. (2) is calculated using FE technique, by analyzing the beam under different loads until the bending stress at the crack tip reaches the flexural strength of the material listed in Table 3. Critical load for each blend of PP/ATH is calculated and mentioned in Table 5. Stress results of the SENB using FE technique are shown in Fig. 14.

Now values of all the variables on right hand side of Eq. (2) are known. By putting all the known values, Eq. (2) gives the fracture toughness (K_{IC}) for each blend of the PP/ATH composite. K_{IC} values for all PP/ATH composites are plotted in Fig. 15 and listed in Table 6. The small values of fracture toughness calculated in this study are near to the general range of fracture toughness of polymers (0.6−5) found in Ref. [15].

Table 5 Critical load for each PP/ATH composites SENB

Blend of PP/ATH	Critical load *P*/N	Geometric factor *Y*
5% ATH	47	10.43858
10% ATH	45	10.43858
15% ATH	38	10.43858
50% ATH	37	10.43858

Table 6 Fracture toughness for various blends of PP/ATH composite

Blend of PP/ATH	Fracture toughness K_{IC}/(MPa·mm$^{1/2}$)	Fracture toughness K_{IC}/(MPa·m$^{1/2}$)
5% ATH	21.28	0.673
10% ATH	20.37	0.644
15% ATH	17.20	0.544
50% ATH	16.75	0.529

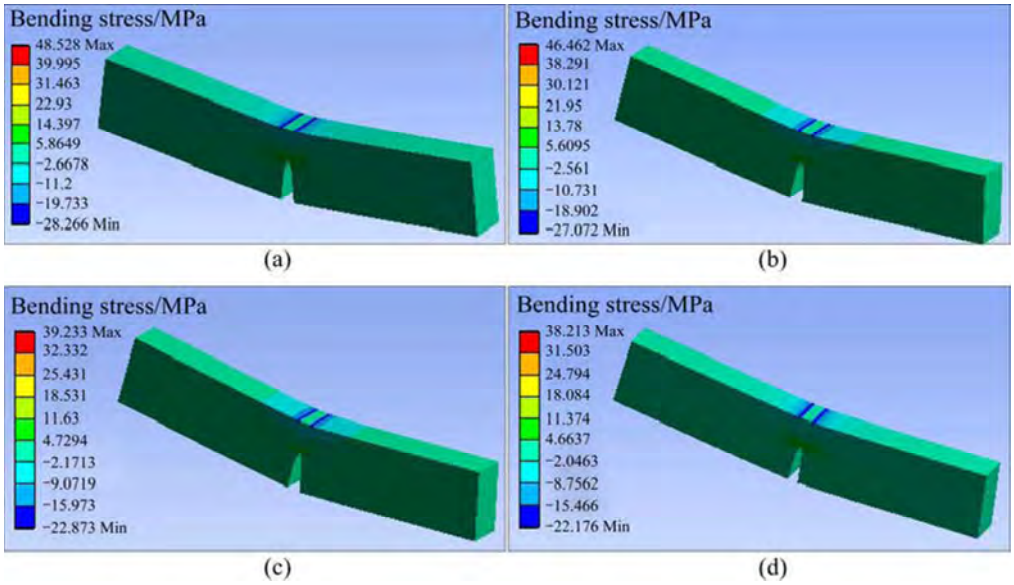

Fig. 14 FE plots of bending stress in SENB of PP/ATH composite of different blends: (a) 5% ATH; (b) 10% ATH; (c) 15% ATH; (d) 50% ATH

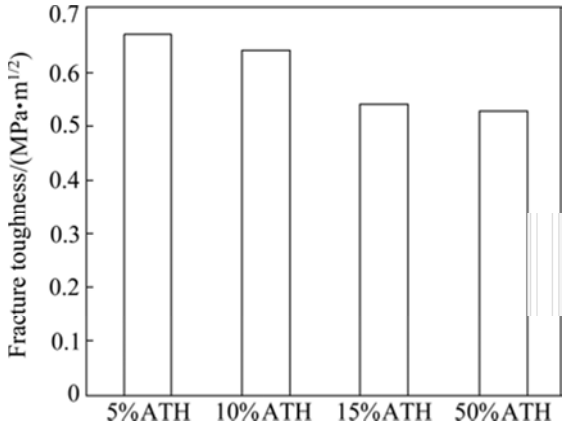

Fig. 15 Variation of fracture toughness with different contents of ATH in PP/ATH composite

7 Conclusion

Mechanical properties including tensile strength, elastic modulus and flexural strength of flame retardant PP/ATH composite are calculated using standard experimental tests and fracture toughness is calculated using finite element technique and ASTM standard formulae. The FE model is validated through the experimental results of three-point bending test and then used to calculate critical load for a notched specimen. After all experimental tests and FE analyses, the comparison graphs for different blends of PP/ATH composite are plotted and all values are tabulated. It is found that tensile strength, flexural strength and fracture toughness of the composite are decreasing with the increase of ATH in the blend. On the other hand, a slight increase in the elastic modulus of the composite has been noted with the increase of ATH. As evident in the literature, addition of ATH may improve the fire retardancy of the PP polymer, but this research has proved that increase in flame retardancy of the composite is on the expense of the mechanical strength.

References

[1] PANDEY J K, REDDY K R, KUMAR A P, SINGH R P. An overview on the degradability of polymer nanocomposites [J]. Polymer Degradation and Stability, 2005, 88(2): 234−250.

[2] ROTHON R N. Particulate-filled polymer composites [M]. UK: Rapra Technology Limited, 2013: 14.

[3] CLIVE M, TERESA C. Polypropylene: The definitive user's guide and databook [M]. New York: Elsevier Science, 2008: 1.

[4] RISTOLAINEN N, HIPPI U, SEPPÄLÄ J, NYKÄNEN A, RUOKOLAINEN J. Properties of polypropylene/aluminum trihydroxide composites containing nanosized organoclay [J]. Polym Eng Sci, 2005, 45: 1568−1575.

[5] FARZAD R H, HASSAN A, PIAH M A M, JAWAID M. Electrical and flammability properties of alumina trihydrate filled polypropylene/ethylene propylene diene monomer composites as insulators in cable applications [J]. Polym Eng Sci, 2014, 54(3): 493−498.

[6] PLENTZ R S, MIOTTO M, SCHNEIDER E E, FORTE M M C, MAULER R S, NACHTIGALL S M B. Effect of a macromolecular coupling agent on the properties of aluminum hydroxide/PP composites [J]. Appl Polym Sci, 2006, 101: 1799−1805.

[7] YENER D O, GUISELIN O, BAUER R. Applications of shaped nano alumina hydrate as barrier property enhancer in polymers: US. 0136744 A1 [P]. 2009−05−28.

[8] BAUER R, BIANCHI C, MIRLEY C L, NOOR S, YENER D. Pigments comprising alumina hydrate and a dye, and polymer composites formed thereof: US. 7479324 B2 [P]. 2009−01−20.

[9] KATZ H S, MILESKI J V. Handbook of fillers for plastics [M]. New York: Springer, 1987: 292−306.

[10] RAMIREZ I, CHERNEY E, JARAYAM S. Silicone rubber and EPDM micro composites filled with silica and ATH [C]// Electrical Insulation and Dielectric Phenomena (CEIDP) 2011

Annual Report Conference, 2011: 20−23.
[11] ZHANG S, HORROCKS A R. A review of flame retardant polypropylene fibres [J]. Prog in Polym Sci, 2003, 28(11): 1517−1538.
[12] TANAKA T, MONTANARI G C, MULHAUPT R. Polymer nanocomposites as dielectrics and electrical insulation-perspectives for processing technologies, material characterization and future applications [J]. Dielectrics and Electrical Insulation, IEEE Transactions, 2004, 11(5): 763−784.
[13] KHALID M, ALI S, ABDULLAH L C, RATNAM C T, CHOONG S Y T. Effect of MAPP as coupling agent on the mechanical properties of palm fiber empty fruit bunch and cellulose polypropylene biocomposites [J]. International Journal of Engineering and Technology, 2006, 3(1): 79−84.
[14] CARNEIRO O S, COVAS J A, VERGNES B. Experimental and theoretical study of twin-screw extrusion of polypropylene [J]. Applied Polymer Science, 2000, 78(7): 1419−1430.
[15] MARK J E. Physical properties of polymers handbook [M]. New York: Springer, 2007: 427.

ATH 浓度对 PP/ATH 复合材料力学性能的影响

Atta ur Rehman SHAH[1], Dong-woo LEE[1], Yi-qi WANG[1], Abdul WASY[1], K. C. HAM[2], Krishnan JAYARAMAN[3], Byung-Sun KIM[4], Jung-Il SONG[1]

1. Department of Mechanical Engineering, Changwon National University, Changwon, Korea;
2. Department of Mechanical Engineering, Inha Technical College, Korea;
3. Department of Mechanical Engineering, University of Auckland, New Zealand;
4. Composite Research Center, Korea Institute of Materials Science (KIMS), Korea

摘　要：ATH 被广泛添加到聚丙烯(PP)中用于制成阻燃复合材料。PP/ATH 复合材料比纯 PP 材料更具防火性。材料中成分的比例最终取决于应用要求。已有文献对这种复合材料的阻燃性能的提高进行了研究，但对机械强度的影响还没有涉及。本文研究了 ATH 浓度对 PP/ATH 复合材料的影响，利用实验测试、ASTM 分析公式和有限元方法研究了材料的拉伸、弯曲和断裂特性。研究结果表明：增加 ATH 对材料的机械强度有不利的影响。

关键词：ATH；聚丙烯；复合材料；防火性；断裂韧性；力学性能

(Edited by Jun ZHAO)